Electron Spin-Polarizability and Charge Dynamics in Ancient Polypeptides – Their Role in Protein Function

Pratik Vyas[1*#§], Kakali Santra[1#], Naupada Preeyanka[1], Anu Gupta[1], Orit Weil-Ktorza[2], Qirong Zhu[1], Liam M. Longo[3,4], Jonas Fransson,[5] Norman Metanis,[2] and Ron Naaman[1*]

[1]Department of Chemical and Biological Physics, Weizmann Institute of Science, Rehovot, 76100, Israel.
[2]Institute of Chemistry, The Hebrew University of Jerusalem, Jerusalem 9190401, Israel
[3]Earth-Life Science Institute, Tokyo Institute of Technology, Tokyo 152-8550, Japan
[4]Blue Marble Space Institute of Science, Seattle, Washington 98104, USA
[5]Department of Physics and Astronomy, Uppsala University, Uppsala 752 36, Sweden

[§]present address: Department of Chemistry, University of Basel, Switzerland

[#]These authors contributed equally to this work

*Corresponding authors:
Ron Naaman: ron.naaman@weizmann.ac.il;
Pratik Vyas: pratikbharat.vyas@unibas.ch

Abstract

We investigated the association of two model primordial polypeptides with DNA, each bearing an ancient and ubiquitous phosphate-binding motif. The association rate and the amount of bound DNA relate to the electron spin-dependent polarizability of the binding polypeptides. The spin-dependence is a result of the chirality of the proteins and is a consequence of the chiral-induced spin selectivity (CISS). We show correlation between the spin dependence and the handedness of the chiral protein. Since the polypeptides studied are hypothesized to be among the initial stand-alone 'seed' fragments from which contemporary protein domains evolved, the results suggest the importance of spin-dependent polarizability early in protein evolution. We propose that the CISS effect played a dominant role in regulating ancient biochemical functions in the context of protein-RNA/DNA world and finally, we provide plausible model-calculations clarifying the underlying reasons for spin selectivity and estimating its impact on protein function.

Introduction

The recognition between proteins and their binding partners is influenced by electrostatic interactions. These interactions stem from charged groups located at or near the binding site that can modulate the diffusion-limited association rate.[1–3] Accordingly, theoretical analyses of protein interactions regularly account for the static charge distributions of protein surfaces.[4] However, it is known that in addition to static charges, the interaction of the protein with any substrate also results in a dynamic charge redistribution in the protein. This redistribution is related to electrical polarizability – the property of a material, including biomolecules, to become polarized in the presence of an electric field. This polarizability stems from both the displacement of charged groups due to the electric field and the redistribution of electronic densities relative to the nuclei. It is important to appreciate that the binding of a protein/enzyme to its cognate ligand/substrate is analogous to applying an electric field to the protein.[5] Indeed, the significance of polarizability in protein structure and activity is increasingly recognized and recent calculations have begun to take it into account.[6–9]

Given the inherent polarizability of proteins, we have recently demonstrated that allosteric effects can occur through charge redistribution in the protein and this charge redistribution depends on the spin of the electrons that are redistributed.[10,11] This electrostatic effect is non-localized, controlled by the withdrawal of charge from sites remote from the active site and redistributed to sites throughout the protein structure. Dubbed charge-reorganization allostery (CRA),[10,11] this form of allostery depends on the spins of the electrons being reorganized, an observation that was attributed to the chiral-induced spin-selectivity (CISS) effect. The CISS effect refers to the experimental observation that the motion of electrons through or within chiral molecules (and materials) depends on their spin state. Which spin is preferred depends on the handedness of the molecule and on the direction of motion of the electrons.[12] While for one handedness the preferred spin will be always pointing parallel to the electron velocity, for the opposite handedness the preferred spin will always point antiparallel to the electron velocity. A consequence of this effect is that the movement of electrons, in a chiral molecule, generates both a charge-polarization (*i.e.*, a separation of positive and negative charges within the molecule and spin-polarization (*i.e.*, a preference for electrons with one specific spin, either "up" or "down") such that one spin has higher density at one electric pole and the other at the opposite pole.[13] The observed spin polarization typically range from 20% to nearly 100% of

the moving electrons. It is important to appreciate that even in chiral systems with closed shell, namely when the total spin is zero, the motion of electrons due to electric field creates uneven spins at the electric poles, so that one spin is associate with the positive pole and the opposite sin with the negative pole. Which spin is associate with which pole depend on the handedness of the system.

As of now numerous studies have demonstrated CISS-effect in physical, chemical and biological systems.[14–16] However, some key, unexplored questions pertain to the origins of CISS in simple, ancient proteins and its significance throughout the history of protein evolution: *Can charge-based allostery and spin selectivity be detected in primitive binding events?* And, if these phenomena are detected, *to what extent could they have promoted or constrained ligand binding by the earliest protein forms?*

Given the structural and functional complexity of modern proteins, the primordial states from which these intricate enzymes evolved are difficult to discern. Recent evidence suggests, however, that many contemporary proteins condensed around relatively short 'seeding' peptides with simple secondary structures, that predated the last universal common ancestor (LUCA).[17–25] These putative evolutionary nuclei – despite billions of years of evolution – have remained largely unchanged on account of their profound functional importance. A prime example of such a peptide is the phosphate-binding loop (P-loop) of ancient and ubiquitous enzyme family P-Loop NTPases that emerged in the protein-RNA world. [23,25–29] Originally, identified in ATP synthases and ATPases, the P-loop is rich in glycine and binds phosphate-containing ligands via the N-terminus of an α-helix, a primitive binding mode.[25] Characterized by the conserved Walker A motif, GxxGxGK(T/S), this functional element binds phosphorylated cofactors such as ATP [30] and DNA [31,32] as well as catalyzes phosphoryl-transfer reactions.[20,30,33,34] Structurally, the P-loop is flanked by a β-strand and an α-helix to form a β-(P-loop)-α motif. This structural β-(P-loop)-α motif is common to various enzyme families and is generally considered to have sparked the emergence of several enzyme families independently.[23,24,35,36]

We have previously described short βα polypeptides (~50 residues) derived from an ancestor inference of theβ-(P-loop)-α motif of P-loop NTPases.[20,32] Despite their simplicity and the lack of auxiliary catalytic residues that are found in contemporary P-loop NTPases, these polypeptides, dubbed P-loop prototypes, demonstrate binding to various phosphorylated-ligands such as ATP, inorganic polyphosphates, and DNA. Moreover, these polypeptides were able to

mediate elementary yet elaborate biochemical reactions such as DNA unwinding and phosphoryl-transfer.[20,32] It is noteworthy that binding to phosphate ligands, including nucleic acids, nucleotides, and nucleotide cofactors, is a fundamental and ancient function.[20–25,32] Therefore, the functions performed by P-loop prototypes not only relate to modern P-loop enzymes, but also hold evolutionary significance and relevance in the context of a primordial world (or preLUCA) world. P-loop prototypes, thus, serve as credible and tangible representations of early 'founder enzymes' and simultaneously function as evolutionary missing links, bridging primitive enzymes and their present-day counterparts. Given the above, *P-loop prototypes and their DNA-binding function presents an ideal experimental system to explore the historical and contemporary significance of electron-spin selectivity in protein function.*

Two P-loop prototypes were selected to investigate the role of charge and electron spin polarization in the phosphate binding: N-αβα and N-βα (**Figures 1A and 1B**).[32] The N-αβα prototype was chosen because its high expression and purification yields, whereas the N-βα construct was chosen because it comprises just the β-(P-loop)-α motif.

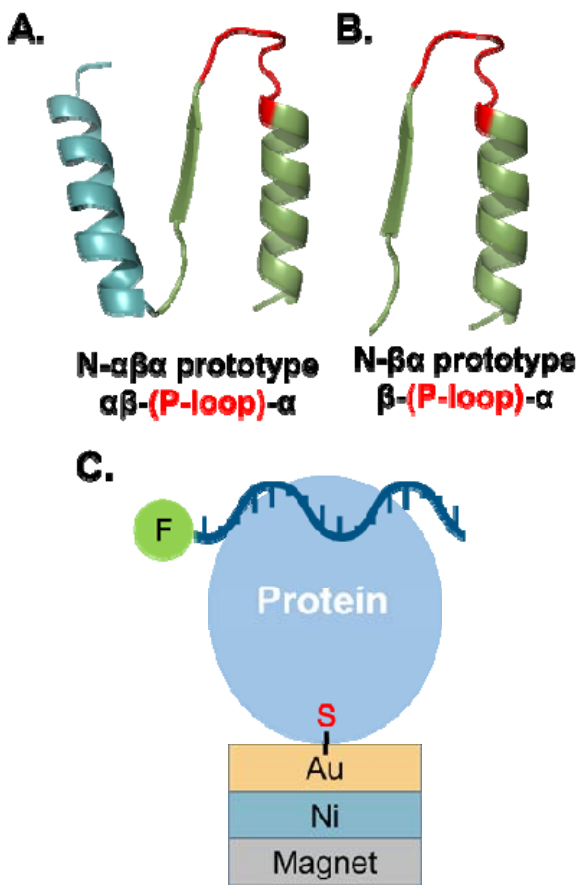

Figure 1: Representative P-loop prototypes and experimental setup. A. The N-αβα prototype comprises the ancestral β-(P-loop)-α motif and one additional α-helix at the N-terminus. **B.** The N-βα prototype comprises only of the ancestral β-(P-loop)-α motif. The structural models in panels A and B depict the ancestrally inferred β1 and α1 in green and the connecting P-loop in red. The additional α-helix in the N-αβα prototype is shown in cyan. The descriptor below each prototype indicates the the order of secondary structure elements (from N- to C-terminus). The prototypes have a propensity to form dynamic oligomers in solution[20,31,32]; therefore, the monomeric models shown here are only schematic depictions. **C.** The experimental setup. Proteins carrying a C-terminal cysteine with a free thiol (-SH) group are adsorbed onto a gold-coated, ferromagnetic nickel layer via an S-Au bond. The ferromagnetic substrates (FM-substrates) with the adsorbed proteins are then placed onto a 0.42T permanent magnet. The entire assembly (magnet + FM-substrates) is transferred to a microscope and binding to fluorescent DNA is

monitored. The experiments were carried out with both orientations of magnet (North or South) facing the substrate. Figure panel **C** was partly created using assets from BioRender.com.

To probe the dependence of DNA-binding on electron spin polarizability, P-loop prototypes were adsorbed onto ferromagnetic substates (FM-substrates) that serves as a source for spin polarized charge. To facilitate the adsorption, a sole cysteine (thiol) residue was incorporated into the prototypes at the C-terminus. Amino acid sequences are provided in **Supplementary Table S2** and substrate preparation is described in the **Methods** section. The immobilization of the prototypes occurred via the formation of sulfur-gold bond between the C-terminal cysteine residue and the gold monolayer on the FM-substrate (**Figure 1C**). The FM-substrates were then placed on a magnet with one polarity facing the substrate and held in place using adhesive tape. Note that the role of the ferromagnetic substrate is only to polarize the spin of the electrons within the Ni/Au substrate and its magnetic field has no direct effect on the protein-DNA binding. Applying an external magnetic field, without having spin polarized substrate, does not affect the DNA-protein binding.

In parallel, a Petri dish containing fluorescent DNA in buffered solution was transferred to the stage of a wide-field microscope. The magnet assembly (*i.e.*, the magnet, substrates, and prototypes) was then inverted onto the Petri dish containing fluorescent DNA and the time-dependent increase in fluorescence intensity was measured. The same process was then repeated with the opposite polarity of magnet facing the substrate (see **Methods**). We will refer to magnet orientations as either UP (North magnet pole facing the FM-substrates) or DOWN (South magnet pole facing the substrates). The orientation of the ferromagnet defines the electron spin that can be injected into the substrate or ejected from the substrate.

Our working hypothesis is structured as follows: when a DNA molecule approaches the binding site of a protein, electrostatic interactions between the two molecules induces a charge reorganization within the protein, *i.e.*, electrons are either accumulated at or repelled away from the binding site. The direction and magnitude of the charge motion depend on the sign and amount of charge on the DNA as well as on the inherent polarizability of the protein. The larger the polarizability of the protein, the more pronounced the charge reorganization induced by DNA at the binding site of the protein will be. It is known that the efficiency of electron injection into the ferromagnet (onto which the proteins are adsorbed) depends on the spin states of the electrons and the magnetization direction of the substrate. Thus, if the charge reorganization

within the protein is spin-dependent – meaning that only electrons with a specific spin are repelled away from the binding site, in accordance with the CISS effect – then for one direction of the magnet relative to the substrate, electrons will be able to be injected into the substrate; however, for the opposite magnetization, electrons will not be injected. Consequently, we anticipate that the polarizability of the protein, and hence its binding affinity to DNA, will vary with the magnetization direction of the substrate. This could lead to a magnetization-dependent and spin-dependent modulation of protein-DNA interactions.

Results

P-loop prototypes exhibit spin-selective function

It was previously demonstrated that the N-αβα prototype showed preferential binding to fluorescently-labeled ssDNA that is rich in thymine and cytosine nucleotides [32] (K_D = 0.67±0.16 μM; hereafter referred as TC-ssDNA, **Supplementary Figure S1; Supplementary Tables S3** and **S4**). Therefore, we used the same DNA for testing the binding of this construct. **Figure 2A** presents adsorption isotherms of TC-ssDNA binding to N-αβα prototype with the magnet pointing towards the molecules (UP) or away from them (DOWN). The resulting time-dependent increase in fluorescence intensity shows that the binding rate and the amplitude of the fluorescence increase (*i.e.*, the amount of prototype-bound DNA) is larger when the ferromagnet is aligned UP (**Figure 2A, Table 1**). To verify that the observed increase in fluorescence is not an artifact of the N-αβα prototype interacting with the fluorophore on the DNA, but rather a consequence of prototype-DNA binding, we measured the adsorption of nuclease-digested TC-ssDNA to the N-αβα prototype-coated substrate. As this sample contains only the free fluorophore and nucleotides, a time-dependent increase in fluorescence would reflect binding to the fluorophore. The fluorescence amplitude of the binding isotherms and the effect of the magnetic field, however, are both small (**Supplementary Figure S2**), consistent with minimal background binding. Next, we examined the binding of ssDNA that is rich in guanines and adenines (henceforth referred to as GA-ssDNA; **Figure 2B**) which has been previously demonstrated to bind relatively weakly to P-loop prototypes[32] (K_D = 1.70±0.68 μM; **Supplementary Figure S1**; **Supplementary Table S3** and **S4**). In this case, when the magnet is pointing UP, the magnitude of GA-ssDNA binding is lower compared to TC-ssDNA and the adsorption (binding) profiles are similar for both magnetic field orientations (*i.e.*, no preference for UP or DOWN orientation, **Figure 2B**).

Spin-selective function is influenced by prototype regions far from spin injection site.

To investigate the role of secondary structure elements on the spin-selective behavior of the prototypes, we tested the binding of the N-βα prototype, that lacks the N-terminal α-helix (**Figure 1B**). The N-βα prototype demonstrated favored binding to TC-ssDNA with the magnet in the UP orientation compared to the DOWN orientation, as is the case of the N-αβα prototype. For the UP orientation, the amplitude of fluorescence increase for TC-ssDNA is greater than the disfavored GA-ssDNA. On the other hand, the binding of GA-ssDNA for both magnet orientations are comparable, indicating decreased spin-selectivity at this magnetic field strength (**Figure 2C**). Thus, similar to N-αβα, the N-βα prototype also shows spin preference. However, the magnetic field effect is notably smaller for the N-βα prototype than it is for the N-αβα prototype, likely owing to the overall weaker binding of this construct (**Figure 2D**).

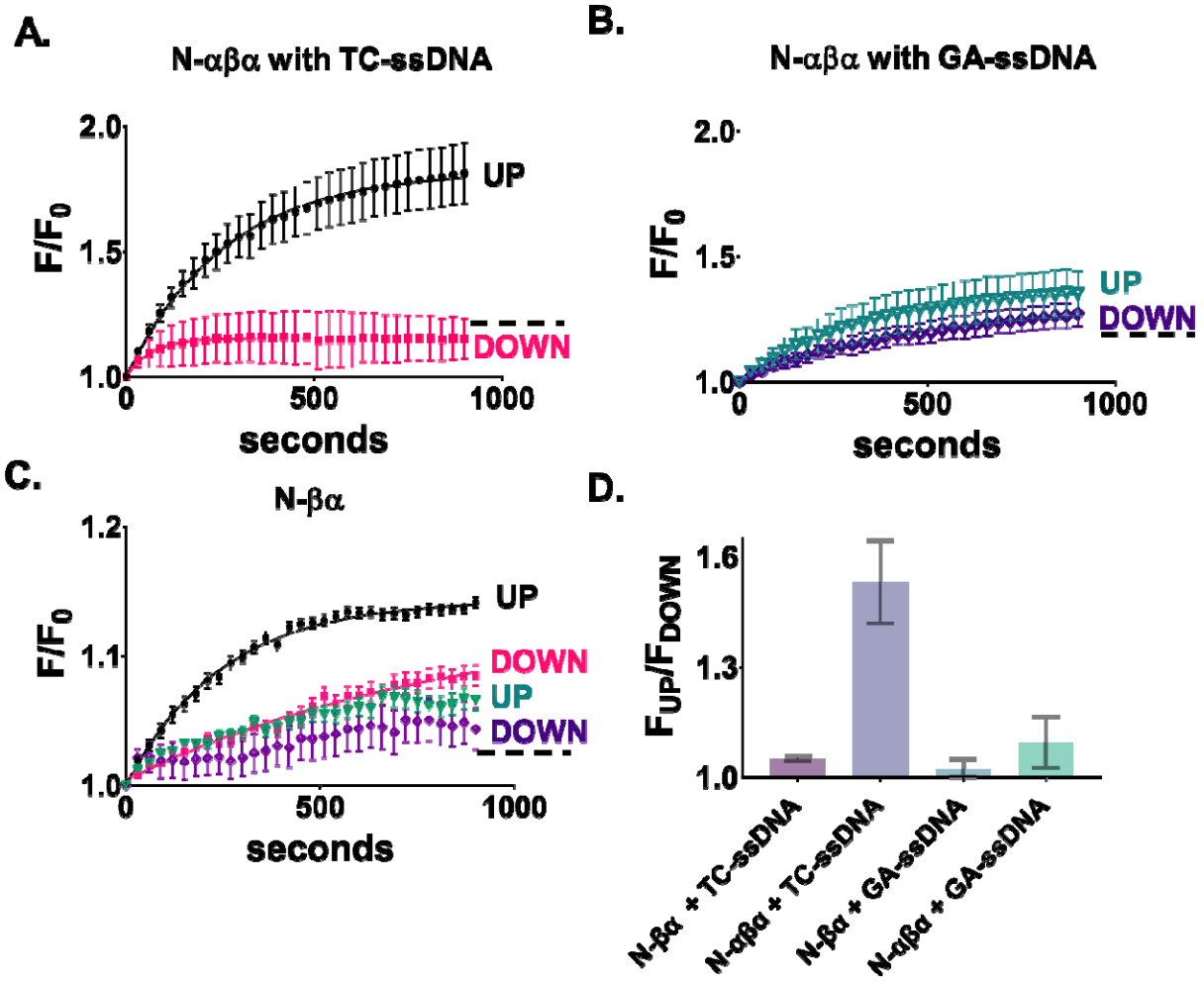

Figure 2: Spin selectivity of DNA binding to N-αβα and N-βα prototypes. Adsorption isotherms showing binding of **A.** TC-ssDNA to N-αβα prototype for UP (black trace) and DOWN (pink trace) orientations and **B.** GA-ssDNA to N-αβα prototype for UP (green trace) and DOWN (purple trace) orientations. **C.** Adsorption isotherms showing binding of N-βα prototype to TC-ssDNA for UP (black trace) and DOWN (pink trace) orientations and to GA-ssDNA for UP (green trace) and DOWN (purple trace) orientations. Fits to data in panels **A**, **B**, and **C** were from a standard one-phase association equation using GraphPad Prism and error bars represent standard deviation from three or four independent measurements. Dotted lines in **A**, **B**, and **C** depict background binding to the free fluorescein (i.e. nuclease digested DNA) (see also **Supplementary Figure S2**) **D.** Relative fluorescence increases. The bar graph displays the relative difference in the endpoint-F/F_0 values corresponding to the binding of each prototype (N-αβα or N-βα) to each DNA sequence (TC-ssDNA or GA-ssDNA). Here, the endpoint fluorescence value of the magnet in the UP orientation, was divided by the endpoint fluorescence value of the magnet in the DOWN orientation, for the same DNA-protein pair (F_{UP}/F_{DOWN}). Error bars represent the standard deviation of three or four independent replicates.

Handedness of terminal cysteine determines spin-selective DNA binding orientation

Next, we determined the relationship between the preferred magnetic orientation and the handedness of the P-loop prototypes. As described earlier, the prototypes have a C-terminal cysteine residue that serves as a 'linker' between the protein and the magnetized FM-substrate – the site for electron injection. N-αβα prototypes that have opposing handedness of the terminal cysteine residue were chemically synthesized. One peptide (N-αβα_LcysEnd) consists of all amino acids in their *L*-form whereas the other peptide (N-αβα_DcysEnd) is identical except for the C-terminal cysteine, which is in the *D*-form (**Supplementary Table S2**). The N-αβα_LcysEnd peptide exhibited spin-selective behavior and a preference for the UP orientation, similar to *E. coli*-expressed N-αβα prototype, which is presumed to contain only *L*-isomers (**Figure 3A**). However, for the N-αβα_DcysEnd peptide, no binding was observed in the UP orientation and stronger binding was observed in the DOWN orientation (**Figure 3B**). Overall, these results indicate spin-selective binding of P-loop prototypes to DNA, influenced by the handedness of the terminal cysteine. These results also show that any potential surface effects related to UP vs. DOWN orientation play no role in the DNA-binding function.

Chiral-inversion reveals spin-dependent charge polarizability as the dominant mechanism in protein-DNA binding

The observed spin selectivity can, in principle, be a result of the spin-dependent charge polarizability within the proteins or due to the spin-dependent interaction between the DNA and the protein. The question of which mechanism is the dominant one can be resolved by studying

the spin-dependent association with proteins that are composed exclusively *L*- or *D*-amino acids, thus inverting the entire handedness of the protein construct (including their DNA-binding sites) and assuming that the binding mode is largely unchanged. To this end, we characterized two model peptides derived from an ancestor sequence reconstruction and amino acid deconstruction[37] of the ancient and ubiquitous helix-hairpin-helix (HhH) family[38] and consisting entirely of either *L*- or *D*-amino acids[39] (see **Supplementary Table S2** for peptide sequences). Despite total chiral inversion (all amino acids changed from *L*- to *D*-form), these peptides have been shown to retain their ability to form coacervates with *D*-RNA.[39] Molecular dynamics simulations suggest that the primary interaction with RNA is mediated by positively-charged side chains,[40] a fact consistent with the observed functional robustness to chiral inversion. **Figures 3D** and **3E** show binding of dsDNA by the HhH peptides *L*-Precursor and *D*-Precursor to a fluorescent 12-bp dsDNA using the same experimental setup described above (**Figure 1C**). **Figure 3D** shows that the *L*-Precursor construct binds dsDNA faster when the substrate is magnetized DOWN than when it is magnetized UP.

In contrast, the *D*-Precursor construct binds faster with the opposite (UP) orientation of the substrate (**Figure 3E**). The rates of binding for the *L*- and *D*-peptides are similar for the favored spins (**Table 1**), suggesting that while spins influence the polarizability of the peptides, resulting in inverted spin preferences for the two enantiomers, the actual rate of binding, once polarizability is maximized, is the same for the two enantiomers. Consequently, the interaction between the DNA and the peptide is not spin dependent, and the observed effect is instead the result of spin-dependent charge polarizability within the protein. This finding supports the conclusion that the interaction is predominantly electrostatic without significant selectivity to the chiral structure.

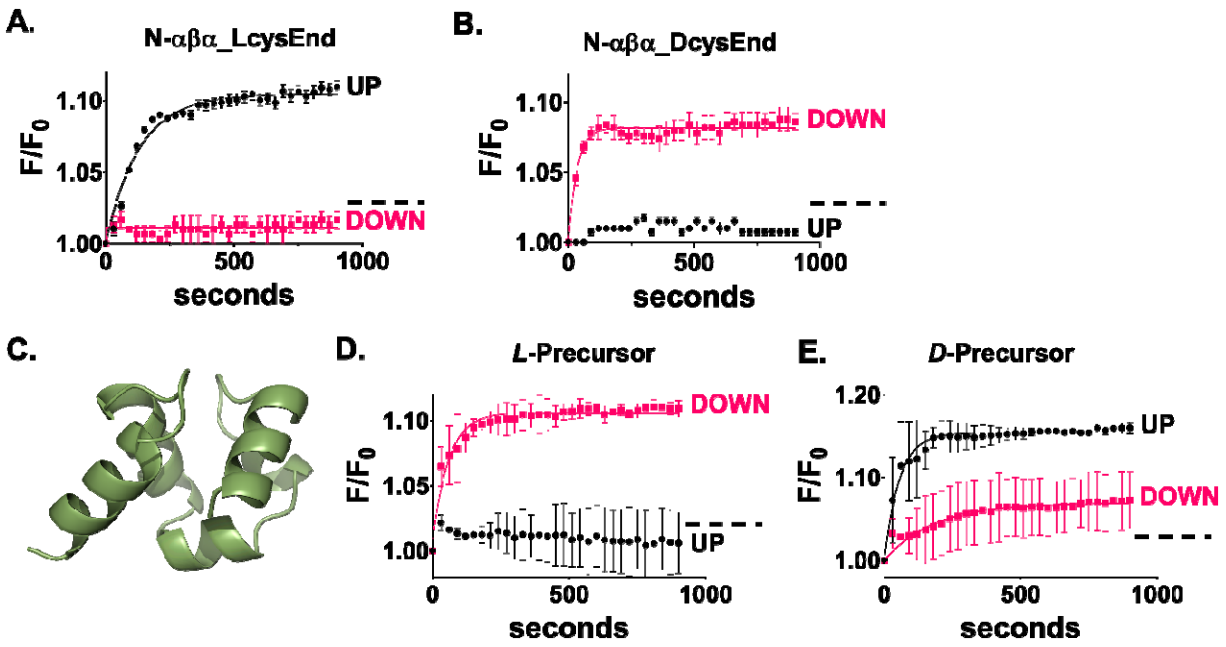

Figure 3: Handedness effect on the magnetism-dependent association. The influence of handedness of synthetic P-loop prototypes and HhH polypeptides on binding to TC-ssDNA or 12-bp dsDNA, respectively, for both magnet orientations. **A.** Adsorption isotherms of TC-ssDNA binding to N-αβα anchored to a ferromagnetic surface via *L*-cysteine (N-αβα_LcysEnd). **B.** Same as A but with N-αβα anchored via *D*-cysteine (N-αβα_DcysEnd). **C.** AlphaFold2 model of the $(HhH)_2$-fold, which is recapitulated upon dimerization of two HhH peptides [40] **D.** Adsorption isotherms of 12-bp dsDNA binding to the Precursor-Arg peptide, which is comprised of a single HhH motif, and for which with all amino acids are in the *L*-form (*L*-Precursor) **E.** Same as **D** but with all amino acids in the *D*-form (*D*-Precursor). Error bars represent standard deviation from three or four independent measurements. Dotted lines in **A**, **B**, **D** and **E** depict background binding of free fluorescein (see also **Supplementary Figure S3**).

Table 1: Apparent rate constants (s^{-1}) of DNA binding to adsorbed P-loop prototypes and HhH polypeptides.

	TC-ssDNA		**GA-ssDNA**	
	UP	**DOWN**	**UP**	**DOWN**
N-αβα	4 (0.1) X 10^{-3} $R^2 = 0.99$	--	3 (0.8) X 10^{-3} $R^2 = 0.98$	--
N-βα	4 (0.2) X 10^{-3} $R^2 = 0.99$	1 (0.2) X 10^{-3} $R^2 = 0.98$	3 (0.1) X 10^{-3} $R^2 = 0.95$	0.7 (0.4) X 10^{-3} $R^2 = 0.88$
N-αβα_LcysEnd	6 (2) X 10^{-3} $R^2 = 0.97$	--		
N-αβα_DcysEnd	--	8 (4) X 10^{-3} $R^2 = 0.98$		
	12-bp dsDNA			
	UP	**DOWN**		

***L*-Precursor**	1.9 (0.1) X 10^{-2} $R^2 = 0.82$	--	
***D*-Precursor**	--	1.8 (0.5) X 10^{-2} $R^2 = 0.76$	

Rate constants (s^{-1}) were determined by fitting the data to a standard one-phase association equation in the GraphPad Prism software (see Methods). Numbers in parenthesis indicates standard deviation from three or four independent measurements. Amino acid sequences are provided in **Supplementary Table S2**. Nucleotide sequences of TC-ssDNA, GA-ssDNA and 12-bp dsDNA are provided in **Supplementary Table S3**. Note that despite a stronger binding for TC-ssDNA, as demonstrated in our previous studies, the association rates observed in the current experiment (which indicates the time taken to reach saturation) are similar, due to high concentrations of protein (dictated by the need to have a uniform monolayer on the FM-substrate) relative to DNA (see 'Methods'). As a result, the binding sites get occupied and the reaction plateaus at a similar rate for both DNA types. The amplitude however is clearly different and greater for the preferred ligand, TC-ssDNA (**Figures 2A and 2B**).

We note that the amplitude of the fluorescence increase (for the test and background controls) in **Figure 2** (i.e. for reactions with biologically purified proteins) is larger than that in **Figure 3** (i.e. for reactions with chemically synthesized constructs). The greater fluorescence signal in **Figure 2** is reproducible upon multiple batches of purification (**Supplementary Figure S4**). This may relate to differences in the oligomeric state adopted by the biologically-produced versus chemically synthesized prototypes. The influence of the histidine tag used for purification of the biologically produced samples may also be a contributing factor in promoting a larger oligomeric form, [29] resulting in greater binding to DNA but also higher non-specific interactions with the hydrophobic dye. Nonetheless, previous studies have shown that the histidine tag does not modulate the function of P-loop prototypes. [31,32] Crucially, the relative preference for the UP orientation for both N-αβα prototype samples remain unchanged, and is opposite to that of the Precursor samples, and the fluorescence signal is significantly above the background in both cases, demonstrating spin-polarizable behavior.

Lastly, as an independent verification of the results obtained using fluorescence microscopy, we performed contact potential difference (CPD) studies with a Kelvin probe [41] (**Figure 4**). These measurements allowed us to confirm the extent of binding for different magnetization directions. The Kelvin probe setup (*Delta Phi Besocke, Jülich, Germany*) was located inside a Faraday cage at ambient conditions. The setup includes a metallic probe electrode (gold grid) placed near the surface of the sample to form a capacitor (**Figure 4A**). The distance between the probe electrode and the surface of the sample is periodically varied to create a frequency dependent capacitance. As a result of the CPD, an AC voltage is generated

across the gap, that is proportional to the difference in the work-function between the sample and the probe electrode. A DC voltage is applied to nullify the AC voltage. A more negative value indicates that the adsorbate reduced the work-function more significantly.

As a representative construct of the proteins described in this study, the N-αβα_LcysEnd construct was adsorbed onto FM-substrates, as with the previous experiments. Substrates were then placed either on unmagnetized substrate or on a permanent magnet with the North polarity facing towards the substrate (UP) or away from the substrate (DOWN). A drop of TC-ssDNA solution (or buffer alone as a control) was the placed onto the adsorbed proteins and incubated for 30 min at room temperature. CPD values were then measured using the setup depicted in **Figure 4A** (see **Methods** for details on the experimental setup and substrate preparation). The results indicate that when the magnet North pole is pointing UP, the work-function becomes less negative (higher work-function) than for adsorption occurring with the magnet pointing DOWN (**Figure 4B**). This means more adsorption of DNA onto the protein-coated surface occurred with the UP configuration. For the surfaces covered with protein only, the CPD values are the most negative. For surfaces covered with protein and DNA, with no magnet, the results are similar to that of the same surfaces with the magnet pointing DOWN. Overall, the Kelvin probe experiment confirms the role of electron-transport in protein function and corroborates the results from fluorescence microscopy.

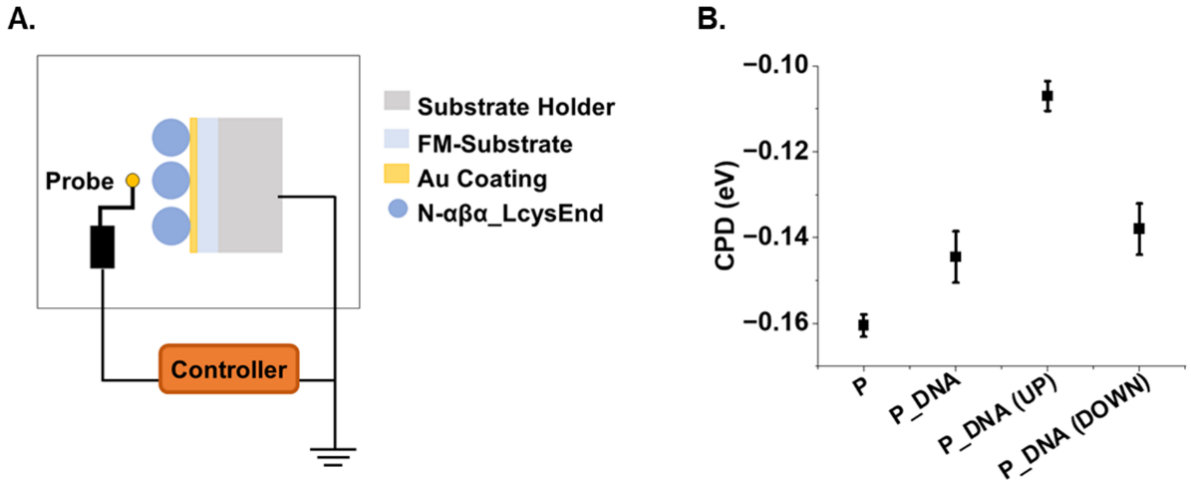

Figure 4. **A.** Schematic of the Kelvin probe setup. **B.** The measured CPD values for the N-αβα_LcysEnd construct. CPD (eV) values were measured for 'Protein-only' (P), adsorbed protein without incubation with DNA; for (P_DNA)', adsorbed protein incubated with DNA with the substrate not magnetized; 'Protein_DNA (UP)', adsorbed protein incubated with DNA with magnet facing towards the protein; and Protein_DNA (DOWN), adsorbed protein incubated

with DNA with magnet facing away from the protein. Error bars represent the standard deviation from four independent experiments.

General discussion

The results indicate that P-loop prototypes and deconstructed HhH peptides demonstrate chiral-induced spin-selective behavior, which in turn governs ligand binding. The extent of the spin-selective effect is highly sensitive to the strength of ligand binding – with only a ~2.5-fold difference in K_D resulting in a near-complete loss of the CISS effect for some protein-ligand pairs – motivating our interest in the role of the CISS effect in primitive biology, where binding affinities may have been weak. More specifically, in the case of P-loop prototypes binding to the TC-rich sequence or of the HhH peptides to dsDNA, the amount of charge that is reorganized is large, and hence charge has to be spread all over the system. However, for GA-rich DNA where the binding to the P-loop prototype is weaker, only a small amount of charge reorganization occurs and, consequently, the charge reorganization is short range and does not result in a significant charge exchange with the substrate (**Figure 2A, 2B**).

The effect of the handedness of the linker residue on DNA binding, provides additional insight into the mechanism of the spin effect (**Figures 3A and 3B**). Schematically, we suggest that when the linker is *L*-Cys it shows the same preference as the native protein, and thus provides a path for the electrons with the preferred spin to move into the ferromagnetic substrate when magnetized UP. For *D*-Cys, on the other hand, electrons with the same spin cannot pass efficiently through the linker and instead accumulate between the linker and the binding site to the DNA, reducing the effective polarizability of the protein. However, if the magnet is pointing DOWN, electrons from the *D*-Cys can now be displaced into the substrate, hence the electrons repelled from the binding site can now be inserted (after their spin is flipped) into the *D*-Cys. The fact that the relative spin orientations between the substrate and the linker, and not the linker and the remainder of the protein, dominates the handedness effect, suggests a clear separation of timescales that will form the basis of future work along with studies to quantify the spin-polarization effects shown in Figures 2 and 3.

Overall, the results show a ~4-fold change in the association rate (**Table 1**) and a significant change in extent of protein-DNA binding based on the direction of the substrate's magnetic field. The dependence is very pronounced, and in some cases, the unfavorable magnetic field direction blocks the association between the DNA and the proteins (see **Figures**

2A, 3A and 3D). When the proteins are made from *D*-amino acids (**Figure 3E**) or the binding to the substrate is through *D*-cysteine (**Figure 3B**), the preferred direction of the magnetic field switches. **Figure 5** schematically presents the mechanism of this effect, which is based on the special properties of chiral systems – the spin-selective transport of electrons via the CISS effect.

Evolutionary implications of spin-selective functions of primordial peptides

We show that protein handedness influences the spin behavior of not only P-loop prototypes, [20,32] but also regulates function of primordial peptides from another ancient protein-motif – the nucleic acid-binding HhH motif (**Figure 3**).[37,38] These peptides are widely accepted to have emerged prior to the emergence of the LUCA and possibly in the protein-RNA/DNA world [21–23,25,31,37,42]. Considering the fundamental and simple nature of this phenomenon, we propose that allosteric interactions based on charge reorganization and chiral-induced electron-spin selectivity represents a plausible contributor to biomolecular recognition early in protein evolution.

Mineral-organic interfaces may have played a crucial role in the functionalization of life and bio-catalysis in the early stages of the earth. [43–45] Binding to minerals has also been shown to preserve protein sequences and accordingly biominerals have been proposed to be excellent source of ancient protein sequences. [46] Minerals and rock surfaces were also likely to have served as compartments and scaffolds for prebiotic reactions and protocells. [47,48] Nickel deposits (the ferromagnetic layer used in our studies) abundant on the Archean earth, [49] played a key role in biological processes, including enzymatic reactions.[50,51] Iron is the most abundant element in the earth's crust and it is postulated to be ubiquitous in the primordial world. [52–55] In a plausible scenario, primordial peptides with both chiralities may have functioned when adsorbed onto mineral interfaces, as described above, or onto magnetite which can provide source of spin-polarized electrons upon UV irradiation. [56,57] Since primordial peptides are unlikely to have a defined tertiary and quaternary structure as their modern counterparts, the CISS effect may have played a dominant role in regulating ancient biochemical functions such as phosphate or nucleic-acid binding [22,23,25]. In line with this, our study shows that, depending on the substrate-magnetization, DNA binding of primordial polypeptides can be entirely abrogated.

While the role of magnet in present study merely allows us to 'observe' the charge-reorganization, it warrants a discussion in context of the primitive Earth. It is true that the magnetic field used in this study to observe the spin-polarization is much stronger than the

magnetic fields present on early earth. However, it has been shown that similar spin-polarizations can be achieved by superparamagnetic magnetite particles, even when they are formed under weak magnetic fields similar to that of the early earth, due to their remnant magnetizations [57,58]. Furthermore, since the effect we describe results from spin-exchange with the substrate, it is the degree of spin-alignment at the protein-substrate (or mineral) interface that is crucial, rather than rather than earth's magnetic field. In other words, the magnetization of naturally occurring minerals is the primary driving force for achieving spin alignment at the protein-substrate (or mineral) interface, rather than the strength of Earth's magnetic field. [57]

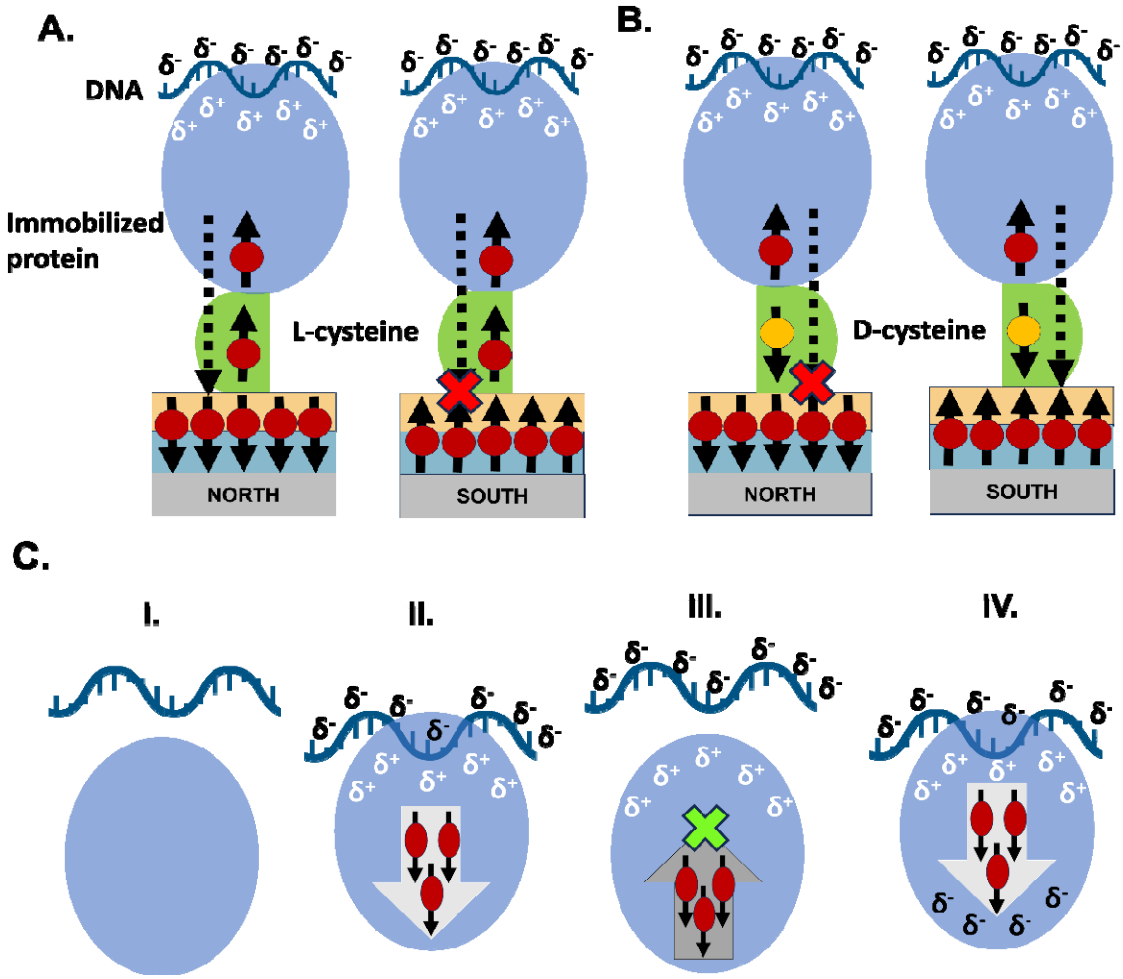

Figure 5: A. Schematic representation of the mechanism of the effect of spin on the protein-DNA interaction. When the spin on the ferromagnet is pointing opposite to the momentary spin of the charge at the interface of the adsorbed proteins (representative spins and electrons migrating trough the protein are shown as black arrow and red ball respectively), charge flows more efficiently between the protein and FM-substrate (shown as dotted arrow penetrating the substrate). This scenario manifests when the North magnet is facing the FM-substrate. When the South magnet is facing the FM-substrate, the spins on the protein and the substrate are pointing the same direction resulting in inefficient electron-flow. **B.** Effect of the *D*-cysteine linker on protein-DNA interaction. The terminal *D*-

cysteine linker, shown in green, which has the opposing chirality to the rest of the protein, flips the direction of spins transmitted through the protein (black arrow, yellow ball). Consequently, the opposite magnet polarity is required to achieve electron-flow, relative to the schematic in A. **C.** Model describing the role of electrons spin-related polarizability in the docking of DNA on the protein. Reaction scheme describes the dynamic interaction of a protein molecule with a DNA molecule to form transient (Protein-DNA)' complex (charge-reorganization step) and the final energetically favored (Protein-DNA) configuration (binding step). **I**. The system before DNA-protein interaction. **II**. The approaching DNA repels electrons with specific spins away from the binding zone. **III**. Upon retraction of the DNA from the protein, the electrons that were withdrawn are not able to flow back because they have the "wrong" spin direction. **IV**. The final docking that results in binding of the DNA to the protein. Figure 5 was partly created using BioRender.com.

What is the significance of electron-spin polarizability for contemporary protein/enzyme systems?

As described below, the importance of spin selectivity is rationalized and supported by a model and simulations (**Figures 5 and 6**). When the DNA approaches the protein adsorbed on the ferromagnet, it induces polarization of the charge in the protein. Here we refer not to the charge localized on specific functional groups, but rather to charge that can be delocalized. This polarization is related to the high frequency polarizability of the protein, or in other terms, to the protein's high frequency dielectric constant. Since the DNA is negatively charged, when it approaches the protein electrons are repelled from the binding site (**Figures 5A, B**). Because of the chirality of the protein, the charge rearrangement depends on the electrons' spin.[13] Namely, electrons with one spin orientation move more efficiently through the protein. If the substrate is magnetized so that the electrons with the preferred spin can be injected into it, then the electrons withdrawn from the binding site can move into the ferromagnet, thereby the effective polarizability of the protein increases. In the specific case of *L*-proteins, this means that since the preferred spin for the electrons' motion is the spin antiparallel to the electrons' velocity, the ferromagnet should be aligned with its North pole pointing towards the protein (namely its majority spin is aligned away from the protein) and therefore the electrons from the protein can be injected into the minority states of the ferromagnet (**Figure 5A**).

The spin dependency of the association is surprising, and the question is if it serves any function in biological systems. In what follows we will present a possible explanation for the importance of the spin. It is well accepted that the "docking" of substrates/ligands on enzymes/proteins is not an abrupt single-step event but a rather a dynamic process, influenced by

the conformational dynamics of the participating biomolecules, involving multiple 'binding-unbinding' events, until the minimum-energy configuration is achieved. [59–63] Upon the first encounter of the DNA and the protein, electrostatic interactions induce charge-reorganization in the protein, *i.e.* due to the approaching negatively charged DNA, electrons are repelled from the binding site in the protein (**Figure 5C, panel II**). As a result of the CISS effect, electrons with spin parallel to their velocity move faster than those with spin aligned antiparallel to their velocity. When the DNA molecules transiently "unbind" from the protein, some of the charge will move back into the binding site, however for these electrons to move back, their spins must flip. This spin-flipping is a relatively slow process that has a lifetime of hundreds of nanoseconds, leading to a delay in the charge returning to its original state (**Figure 5C, panel III**). As a result, DNA molecules are attracted back towards the protein. This dynamic enhances their binding affinity to the protein and prevents the complete unbinding of DNA before a minimal energy conformation is reached (**Figure 5C, panel IV**).

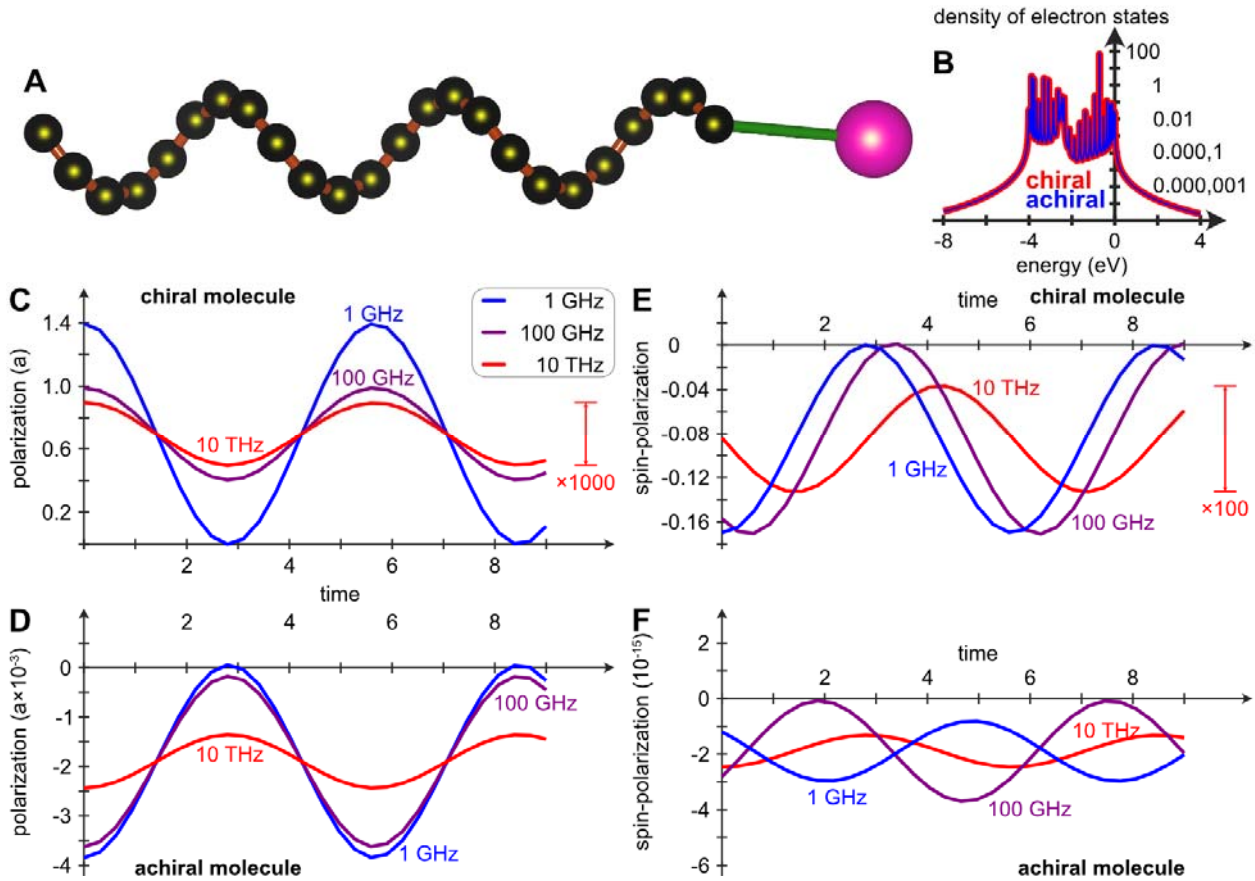

Figure 6: A. Schematic of the chiral system (black balls, brown bonds) connected to the external charge (magenta ball, green coupling). The corresponding achiral system is represented by a zig-

zag chain of sites. **B**. Density of electron states for the chiral (red) and achiral (blue) molecules. The chemical potential is set to 0. **C**. & **D**. Time-dependent variations of the dominant component of the electric polarization vector $\boldsymbol{P}$ for the **C**. chiral and **D**. achiral system, under the time-dependent coupling between the system and external charge. The time-dependent coupling varies harmonically with frequencies $\nu_0 = 1$ GHz, 100 GHz, 10 THz. Results with more frequencies are presented in the supplementary information. **E**. & **F**. Time-dependent variations of the spin-polarizations corresponding to the polarizations in **C**. & **D**. The sites in the system host electron levels at $\epsilon_m = -2t_0$ and are elastically coupled by the nearest neighbor coupling $t_0 = 1$ eV and next-nearest neighbor coupling $\lambda_0 = 1$ meV, whereas the inelastic coupling strengths are $t_1 = t_0/10$ and $\lambda_1 = \lambda_0/10$. The system vibrates with the frequency corresponding to the energy $\omega_0 = 0.5$ eV, the helix radius a $= 5$ Å, and the temperature is set to $T = 300$ K.

For testing if the proposed mechanism can in principle take place, we performed quantum simulations to model the dynamics of the charge density with a model system, comprising of a chain of $\mathbb{M}$ sites distributed in helical (chiral) or a zig-zag (achiral) shape (Figure 6A). We shall refer to these model systems as the chiral and achiral molecules. Each site may hold an electron at the energy ε_m and is coupled to its nearest and next-nearest neighbor by both elastic (t_0, λ_0) and inelastic (t_1, λ_1) components, where the inelastic components account for nuclear vibrations that are coupled to the electronic charge (t_1) and to the electronic spin through the vibrationally enhanced spin-orbit coupling (λ_1). The chiral or achiral structures are controlled by the next-nearest neighbor interaction. The effect of the perturbing charge on the chiral system is provided by an additional external electron, illustrated by the magenta ball in **Figure 6A**, where the green line between this charge and the system signifies the (time-varying) electrostatic coupling between the DNA and the protein. The details of setting up the molecule can be found in the Supplementary Information and in Refs. 64,65.

The simulations of the charge dynamics in the chiral and achiral chain are undertaken by varying the coupling between the external charge and the system harmonically as $U_0(1 + \cos \nu_0 t)$, where U_0 defines the maximum coupling strength, ν_0 the frequency of the variations, and t is the time. The method used for the simulations of the dynamics is described in the Supplementary Information and in Ref. 65.

In Figure 6B, we have plotted the density of electron states for the chiral and achiral molecules. The spectrum, which is confined below the chemical potential, zero vertical line, should be considered as the set of occupied orbitals whereas the unoccupied orbitals are assumed to be located at energies beyond 4 eV. It should be noticed that the densities for the two molecules are identical.

By the time-dependent variations in the local charge conditions near one of the edges of the system that models the molecule (protein), the internal charge of the molecules forced to react in response to these changes. As a measure of the variations, we calculate the electric polarization vector $P = (Px, Py, Pz)$ of the system with respect to its center of mass. In both types of molecules, there is a distinctive time-dependence imposed on the charge polarization (**Figure 6C** and **6D**), where largest vector component of P is plotted as function of time. Here, we compare the dynamical responses for frequencies between 1 MHz and 10 THz, and the responses are plotted on the same unit less time axis to enable a comparison.

First, one can notice that the overall polarization is stronger in the chiral than in the achiral structure, both in amplitude and mean value. Second, it can be seen that the time-dependent variations tend to be strongly suppressed with in increasing frequency in the chiral structure compared to the achiral one. In the chiral molecule, there is a clear trend of decreasing amplitude in the temporal response the higher the frequency, a trend which cannot be discerned in the achiral molecule.

In **Figure 6E** and **6F** we also plot the associated time-dependent spin-polarization for the chiral and achiral molecules, respectively, and there are two striking differences between the induced spin-polarizations. First, while there is a significant dynamical spin-polarization in the chiral molecules, there is none at all in the achiral (notice that the vertical scale is in units of 10^{-15}). Second, for the chiral molecule, also the spin-polarization tends to become increasingly time-independent with increasing frequency, whereas there are hardly any changes in the achiral molecule.

The results from the calculations clearly point to that the electric and spin polarizations are intimately related in chiral molecules, while these quantities may be considered as independent in achiral. This conclusion can be drawn from three observations. First, since the densities of electron states in the two molecules are identical (**Figure 6B**), one can effectively exclude the possibility that the responses to the time-dependent perturbation would be a density effect. Second, since the chiral molecule develops a spin-polarization whereas the achiral does not, in response to the time-dependent perturbation, we can deduce that the induced spin-polarization is the key quantity that is distinct between the two molecules. Third, the fact that the spin-polarization in the chiral molecule becomes increasingly time-independent at a non-vanishing mean value with increasing frequency (**Figure 6E**), indicates that charges with

different spins accumulate in different spatial locations and that there is a spatial imbalance built up through this differentiation of the spin. This spatial imbalance can, hence, be detected as an electric polarization (**Figure 6C**).

It is important to appreciate that interaction of protein with any binding-partner will involve charge-reorganization within the protein, due to the different electrochemical potentials of the protein and the binding-partner. Hence, an electron with the preferred spin, which is pushed away by the external charged ball (the DNA in our experimental system), gives rise to a positive charge polarization. Restoration of the charge distribution as the DNA moves away from the protein, during the docking process, requires a spin flip of the accumulated charge. However, this spin-flip requires additional time to occur, time under which the DNA has changed its motion and is again moving towards the protein. As a result, the internal charge dynamics of the protein is quenched and the polarization, therefore, remains positive and nearly constant despite the motion of the external charge. Hence, the mechanism described above should be relevant to all association processes, in which the objects are chiral.

Overall, we have demonstrated that the association between model primordial polypeptides and DNA depends on electron spin. The spin dependence is proven by the dependence of the association on the direction of the spin polarization in the ferromagnetic substrate. We also showed that the effect of the spin depends on the handedness of the protein. For *L* protein the enhancement is with one spin while for *D* protein it is with the opposite spins. We performed model calculations aiming at demonstrating the proposed mechanism for the spin effect. The relatively simple model that does include spin-vibration and electron-electron interactions indicates that the mechanism proposed for the spin effect in the reaction follows the basic physical properties. It is also important to realize that a full “realistic” calculation is beyond the current state of the art calculations.

We believe that the calculated model, although simplified, includes all the essential ingredients of the physical process. The model, in conjunction with the experimental results, presents, in a very clear way, the difference between chiral and achiral systems and the role of the electron’s spin in making this difference. The spin effect is a result of the polarizability of the protein being spin selective due to the chiral-induced spin-selectivity (CISS) effect. The CISS effect relates homochirality (be it *L* or *D*) to the spin-dependent polarization of electrons which, in turn, influences internal charge dynamics. Therefore, there is a direct relation between

homochirality and the charge dynamics within proteins that affect their function. We propose that the spin selectivity enhances the binding rate between protein and substrate by elongating the relaxation time of the 'chiral-induced electric dipole' moment in the protein. If true, spin selectivity may have promoted the emergence of homochirality.

In conclusion, our study provides evidence of CISS-effect regulating functions in tangible, primordial protein systems, thus highlighting an underappreciated consequence of homochirality that may have helped shape nascent biological systems.

Materials and Methods

DNA and cloning. The synthetic gene fragments encoding P-loop prototypes were sourced from *Twist Biosciences* and inserted into a pET29(+)b expression vector using standard restriction free cloning method. Similarly, mutant prototypes were generated using standard site-directed mutagenesis via restriction-free cloning with primers obtained from *Integrated DNA Technologies* (IDT).

Protein expression and purification. P-loop prototypes have a C-terminal tag that comprises of a Trp residue for concentration determination by measuring absorbance at 280 nm (the prototypes are devoid of aromatic residues) followed by 6xHis for purification (DNA and amino acid sequences are provided in **Supplementary Tables S1 and S2**). Following purification, the yield and purity of purified proteins was assessed by SDS-PAGE. Typically, four peak elution fractions (total 7.5 ml) were pooled together and subjected to two rounds of dialysis (two hours at room temperature plus overnight at 4 °C) in buffer containing 50 mM Tris and 100 mM NaCl (pH 8) to dialyze out the imidazole. The proteins generally precipitated during the dialysis step and required an osmolyte such as L-arginine to resolubilize the proteins. The samples were centrifuged; the protein pellet was collected and dissolved in buffer containing 50 mM Tris (pH 8), 100 mM NaCl and 1 M L-arginine (osmolyte to resolubilize the proteins). Purified prototypes, stored in this buffer at 4 °C, at 100 to 200 μM concentrations, remained soluble and active for periods of ten-fourteen days.

Peptides. Synthetic peptide constructs of N-αβα prototype harboring all *L*-amino acids (N-αβα_LcysEnd) and harboring all *L*-amino acids except for the terminal cysteine in *D*-form (N-αβα_DcysEnd) were procured from *Synpeptide*. Peptides were dissolved in 10% Acetonitrile + 90% Millipore water according to manufacturer's instructions at 2.5 mM stock concentrations.

HhH peptides were synthesized inhouse (**Supplementary Figure S5**; see 'Supplementary Methods' for details). Peptides were divided into aliquots and stored at -20 ºC till further use.

Preparation of the ferromagnetic substrate. Ferromagnetic substrates were prepared as described previously [66]. An 8-nm thick Ti adhesive layer was deposited on a p-type (boron-doped), silicon (Si) ⟨100⟩±0.9° wafer. Next, a 100-nm-thick nickel (Ni) layer, that serves as ferromagnetic layer, was deposited on the adhesive coated Si wafer using an electron beam evaporator. The Ni layer was coated with a thin gold (Au) layer of 5 nm. The evaporator chamber was kept at high vacuum ($<10^{-7}$ Torr) and ambient temperature during deposition of the metal layers. Substrates were cut into 23 × 23 mm^2 squares using diamond cutter for all microscopy experiments. The substrate pieces were cleaned by boiling in acetone for 10 mins, followed by boiling in ethanol for 10 mins and 1 min sonication in water-bath to dislodge any broken debris from the surfaces.

Drop casting/adsorbing proteins on ferromagnetic substrates. P-loop prototype proteins were diluted and dialyzed into 50 mM tris buffer (pH =8), to a final concentration of 100 μM. A ten-fold molar excess of TCEP was added to the proteins or peptides to reduce the terminal cysteines. The samples were kept at room temperature (for biologically purified proteins) or on ice (for synthetic peptides) for 3 hrs. to ensure complete reduction of all cysteine residues. The samples were filtered using BioRad *Micro Bio-Spin* P-6 columns to remove TCEP. The protein concentration was checked using a nanodrop and final concentration was adjusted to 80 μM.

The HhH peptides are dissolved in a 50 mM Tris buffer, 150 mM NaCl (pH =7.5). The final concentration of the peptides was 20 μM and it was verified using Nanodrop. Five times concentrated TCEP solution was added to avoid the formation of disulfide bonds between the peptides. Peptides were filtered using spin columns as above.

Boiled and cleaned surfaces from cleaning step described above, were dried using inert N_2 gas-gun, one at time and immediately drop-casted with 30 μL of protein sample in the center of each substrate. The substrates with drop-casted proteins were placed in a petri-dish, sealed with a parafilm and placed overnight (16 hr.) at room temperature (for biologically purified proteins) or at 4 degrees (for synthetic peptides).

Hybridization of the dsDNA for the binding kinetics experiments. The dsDNA solution was prepared by mixing the two complementary strands of ssDNA in 0.4 M phosphate buffer at pH 7.2, followed by PCR thermal incubation (60 °C for 10 min, then cooled down to 15 °C at the rate of -1 °C per min). The solution was then filtered by a Micro Bio-Spin P-30 column. The absorption of the solution was measured and diluted to final concentration of 1 μM.

Preparing substrates for microscopy experiments. Monolayer formation from overnight (16 hr.) incubation of proteins with Au-coated substrates was carried out using Polarization modulation-infrared reflection-adsorption spectroscopy (PM-IRRAS) and atomic force microscopy (see '**Supplementary Methods'**, **Supplementary Figures S7, S8 and S9 respectively**). Overnight incubated FM-substrates were washed thrice with 1 mL of 50 mM Tris buffer (pH =8). A small scratch, using a diamond cutter was created at the center of each substrate. By locating the scratch in the microscopy experiments (discussed later) allowed us to ensure uniformity across experiments by image the center of substrates.

Microscopy measurements. We measured the binding kinetics of the ssDNA to P-loop prototypes or dsDNA to HhH peptides anchored on FM-substrates (described above) using a ZEISS Axio-Observer.Z1 inverted fluorescence widefield microscope. Prepared substrates were then placed on to a permanent 0.42 T magnet, held in place using an adhesive tape, with the North Pole facing the substrate. In parallel, a drop of 80 μL fluorescently labeled (6-FAM) ssDNA or dsDNA placed at the center of the 35 mm, glass-bottom-well, Petri dish (*MAKTEK)*, which was then transferred to the microscope stage. The assembly of the magnet with FM-substrate was then inverted onto the Petri dish containing fluorescent DNA solution.

Images were acquired using a 40× air objective lens (LD Plan-Neofluar. 40x / 0.6). Using a GFP filter, the emitted fluorescence was collected and was separated from the excitation beam by placing two dichroic beam splitters in the optical path. It was then routed to an avalanche photodiode (APD) for fluorescence imaging. Before initiating test experiments, a control experiment was carried out to focus the z-position at the surface–solution interface. This was done by locating the scratch on the FM-substrate described earlier allowed. This z-position was then fixed for all the experiments. Experiments were initiated and fluorescence intensity images were acquired using *Slidebook* software for every 30s for a duration of 15 mins. We selected the same region from each image with a size of 400 pixels × 400 pixels, located with the help of the

scratch. The increase in fluorescence relative to initial fluorescence value (F/F_0) was calculated and plotted versus time. Each experiment was repeated three times to ensure the reproducibility of the results. The errors shown in the plots were calculated as the standard deviation from the mean. The entire procedure was then repeated with the South magnet pointing towards the substrate.

The F/F_0 values were then fitted to one-phase association equation (eq. 1) in GraphPad Prism software to derive rate constants.

$$Y = Y_0 + (Plateau - Y_0) \times (1 - exp(-k \times X)) \qquad \text{(eq. 1)}$$

Where Y_0 is the F/F_0 value at time zero, $Plateau$ is the F/F_0 value at time t (at saturation) and k is the rate constant expressed in inverse time (s^{-1}) units (listed in Table 1).

Macroscopic Contact Potential Difference (CPD) measurements. The CPD measurements were performed using a commercial Kelvin probe set up (Delta Phi Besocke, Jülich, Germany) confined inside a Faraday cage under atmospheric pressure. A general kelvin probe set up includes a metallic probe electrode (gold grid) which is placed near the surface of the sample to form a capacitor (**Figure 4A**). The distance between the probe electrode and the surface of the sample is periodically varied to create a frequency dependent capacitance. Now an AC voltage is generated across the gap, and this is proportional to the voltage difference between the sample and the probe electrode. Rather than measuring AC voltage directly, a DC voltage is generally applied (to nullify the response) which measures the CPD. The CPD signal is allowed to stabilize before recording.

Substrate preparation for CPD measurements. The substrates were p-doped silicon wafers Si⟨100⟩ upon which Ti/Ni/Au- 8nm/60nm/8nm with 0.3Å/sec, 0.5Å/sec, and 0.3Å/sec deposition rate at 10^{-8} Torr pressure were grown by an electron beam evaporator. After deposition, the substrates were cleaned with boiling acetone followed by boiling ethanol for 15 minutes each. Immediately after the cleaning, the substrates were dried under nitrogen flow. In parallel, the N-αβα_LcysEnd peptides were incubated with TCEP for reduction of the terminal cysteine as described in earlier section (see *Drop casting/adsorbing proteins on ferromagnetic substrates*). The peptides were purified of TCEP and drop casted on the clean-dried substrates and incubated for 16 hours at 4 ^{0}C temperature. Substrates were washed thrice with 50 mM Tris buffer (pH 8) solution, dried with inert nitrogen gas, and placed on a permanent magnet with

either the North polarity facing the substrate (UP) or away from the substrate (DOWN). A drop of TC-ssDNA (same DNA that is used for microscopy experiments) was placed onto the substrates and incubated for 30 minutes. The DNA is then aspirated out with a pipette, dried under nitrogen flow and then CPD measurements were conducted.

References

1. Schreiber, G. & Fersht, A. R. Rapid, electrostatically assisted association of proteins. *Nat. Struct. Biol.* **3**, 427–431 (1996).
2. Sheinerman, F. B., Norel, R. & Honig, B. Electrostatic aspects of protein-protein interactions. *Curr. Opin. Struct. Biol.* **10**, 153–159 (2000).
3. Bauer, M. R. & Mackey, M. D. Electrostatic Complementarity as a Fast and Effective Tool to Optimize Binding and Selectivity of Protein–Ligand Complexes. *J. Med. Chem.* **62**, 3036–3050 (2019).
4. Schreiber, G., Haran, G. & Zhou, H.-X. Fundamental Aspects of Protein−Protein Association Kinetics. *Chem. Rev.* **109**, 839–860 (2009).
5. Fried, S. D., Bagchi, S. & Boxer, S. G. Extreme electric fields power catalysis in the active site of ketosteroid isomerase. *Science* **346**, 1510–1514 (2014).
6. Khoruzhii, O. *et al.* Application of a polarizable force field to calculations of relative protein-ligand binding affinities. *Proc. Natl. Acad. Sci. U. S. A.* **105**, 10378–10383 (2008).
7. Lopes, P. E. M. *et al.* Force Field for Peptides and Proteins based on the Classical Drude Oscillator. *J. Chem. Theory Comput.* **9**, 5430–5449 (2013).
8. Halgren, T. A. & Damm, W. Polarizable force fields. *Curr. Opin. Struct. Biol.* **11**, 236–242 (2001).
9. Jing, Z. *et al.* Polarizable Force Fields for Biomolecular Simulations: Recent Advances and Applications. *Annu. Rev. Biophys.* **48**, 371–394 (2019).
10. Banerjee-Ghosh, K. *et al.* Long-Range Charge Reorganization as an Allosteric Control Signal in Proteins. *J. Am. Chem. Soc.* **142**, 20456–20462 (2020).
11. Ghosh, S. *et al.* Substrates Modulate Charge-Reorganization Allosteric Effects in Protein-Protein Association. *J. Phys. Chem. Lett.* **12**, 2805–2808 (2021).
12. Naaman, R., Paltiel, Y. & Waldeck, D. H. Chiral Induced Spin Selectivity and Its Implications for Biological Functions. *Annu. Rev. Biophys.* **51**, 99–114 (2022).
13. Kumar, A. *et al.* Chirality-induced spin polarization places symmetry constraints on biomolecular interactions. *Proc. Natl. Acad. Sci. U. S. A.* **114**, 2474–2478 (2017).
14. Bloom, B. P., Paltiel, Y., Naaman, R. & Waldeck, D. H. Chiral Induced Spin Selectivity. *Chem. Rev.* **124**, 1950–1991 (2024).
15. Fransson, J. The Chiral Induced Spin Selectivity Effect What It Is, What It Is Not, And Why It Matters. *Isr. J. Chem.* **62**, e202200046 (2022).
16. Yang, C. *et al.* Real-time monitoring of reaction stereochemistry through single-molecule observations of chirality-induced spin selectivity. *Nat. Chem.* **15**, 972–979 (2023).
17. Eck, R. V & Dayhoff, M. O. Evolution of the structure of ferredoxin based on living relics of primitive amino Acid sequences. *Science* **152**, 363–366 (1966).
18. Jayaraman, V., Toledo-Patiño, S., Noda-García, L. & Laurino, P. Mechanisms of protein evolution. *Protein Sci.* **31**, e4362 (2022).
19. Berezovsky, I. N. Towards descriptor of elementary functions for protein design. *Curr.*

Opin. Struct. Biol. **58**, 159–165 (2019).
20. Vyas, P., Malitsky, S., Itkin, M. & Tawfik, D. On the Origins of Enzymes: Phosphate-Binding Polypeptides Mediate Phosphoryl Transfer to Synthesize Adenosine Triphosphate. *J. Am. Chem. Soc.* **145**, 8344–8354.
21. Söding, J. & Lupas, A. N. More than the sum of their parts: On the evolution of proteins from peptides. *BioEssays* **25**, 837–846 (2003).
22. Ma, B.-G. *et al.* Characters of very ancient proteins. *Biochem. Biophys. Res. Commun.* **366**, 607–611 (2008).
23. Alva, V., Söding, J. & Lupas, A. N. A vocabulary of ancient peptides at the origin of folded proteins. *Elife* **4**, 1–19 (2015).
24. Longo, L. M. *et al.* On the emergence of P-Loop NTPase and Rossmann enzymes from a Beta-Alpha-Beta ancestral fragment. *Elife* **9**, e64415 (2020).
25. Longo, L. M., Petrović, D., Kamerlin, S. C. L. & Tawfik, D. S. Short and simple sequences favored the emergence of N-helix phospho-ligand binding sites in the first enzymes. *Proc. Natl. Acad. Sci.* **117**, 5310 LP – 5318 (2020).
26. Saraste, M., Sibbald, P. R. & Wittinghofer, A. The P-loop — a common motif in ATP- and GTP-binding proteins. *Trends Biochem. Sci.* **15**, 430–434 (1990).
27. Lupas, A. N., Ponting, C. P. & Russell, R. B. On the evolution of protein folds: are similar motifs in different protein folds the result of convergence, insertion, or relics of an ancient peptide world? *J. Struct. Biol.* **134**, 191–203 (2001).
28. Leipe, D. D., Wolf, Y. I., Koonin, E. V. & Aravind, L. Classification and evolution of P-loop GTPases and related ATPases. *J. Mol. Biol.* **317**, 41–72 (2002).
29. Leipe, D. D., Koonin, E. V. & Aravind, L. Evolution and classification of P-loop kinases and related proteins. *J. Mol. Biol.* **333**, 781–815 (2003).
30. Walker, J. E., Saraste, M., Runswick, M. J. & Gay, N. J. Distantly related sequences in the alpha- and beta-subunits of ATP synthase, myosin, kinases and other ATP-requiring enzymes and a common nucleotide binding fold. *EMBO J.* **1**, 945–951 (1982).
31. Romero Romero, M. L. *et al.* Simple yet functional phosphate-loop proteins. *Proc. Natl. Acad. Sci.* **115**, E11943 LP-E11950 (2018).
32. Vyas, P. *et al.* Helicase-Like Functions in Phosphate Loop Containing Beta-Alpha Polypeptides. *Proc. Natl. Acad. Sci.* **118**, (2021).
33. Knowles, J. R. Enzyme-Catalyzed Phosphoryl Transfer Reactions. *Annu. Rev. Biochem.* **49**, 877–919 (1980).
34. Lassila, J. K., Zalatan, J. G. & Herschlag, D. Biological phosphoryl-transfer reactions: understanding mechanism and catalysis. *Annu. Rev. Biochem.* **80**, 669–702 (2011).
35. Gruic-Sovulj, I., Longo, L. M., Jabłońska, J. & Tawfik, D. S. The evolutionary history of the HUP domain. *Crit. Rev. Biochem. Mol. Biol.* 1–15 (2021) doi:10.1080/10409238.2021.1957764.
36. Longo, L. M., Hirai, H. & McGlynn, S. E. An evolutionary history of the CoA-binding protein Nat/Ivy. *Protein Sci.* **31**, e4463 (2022).
37. Longo, L. M. *et al.* Primordial emergence of a nucleic acid binding protein via phase separation and statistical ornithine to arginine conversion. *Proc. Natl. Acad. Sci.* **117**, 15731–15739 (2020).
38. Doherty, A. J., Serpell, L. C. & Ponting, C. P. The Helix-Hairpin-Helix DNA-Binding Motif: A Structural Basis for Non-Sequence-Specific Recognition of DNA. *Nucleic Acids Res.* **24**, 2488–2497 (1996).

39. Weil-Ktorza, O. *et al.* Functional Ambidexterity of an Ancient Nucleic Acid-Binding Domain. *bioRxiv* 2023.03.06.531422 (2023) doi:10.1101/2023.03.06.531422.
40. Seal, M. *et al.* Peptide-RNA Coacervates as a Cradle for the Evolution of Folded Domains. *J. Am. Chem. Soc.* **144**, 14150–14160 (2022).
41. Ghosh, S. *et al.* Effect of Chiral Molecules on the Electron's Spin Wavefunction at Interfaces. *J. Phys. Chem. Lett.* **11**, 1550–1557 (2020).
42. Koonin, E. V, Wolf, Y. I. & Aravind, L. Protein fold recognition using sequence profiles and its application in structural genomics. *Adv. Protein Chem.* **54**, 245–275 (2000).
43. Hazen, R. M. & Sverjensky, D. A. Mineral Surfaces, Geochemical Complexities, and the Origins of Life. *Cold Spring Harb. Perspect. Biol.* **2**, (2010).
44. Stephenson, J. D., Popović, M., Bristow, T. F. & Ditzler, M. A. Evolution of ribozymes in the presence of a mineral surface. *RNA* **22**, 1893–1901 (2016).
45. Hazen, R. M. Chance, necessity and the origins of life: a physical sciences perspective. *Philos. Trans. R. Soc. A Math. Phys. Eng. Sci.* **375**, 20160353 (2017).
46. Demarchi, B. *et al.* Protein sequences bound to mineral surfaces persist into deep time. *Elife* **5**, e17092 (2016).
47. Fontecilla-Camps, J. C. Primordial bioenergy sources: The two facets of adenosine triphosphate. *J. Inorg. Biochem.* **216**, 111347 (2021).
48. Gözen, I. *et al.* Protocells: Milestones and Recent Advances. *Small* **18**, 2106624 (2022).
49. Bekker, A. *et al.* Atmospheric Sulfur in Archean Komatiite-Hosted Nickel Deposits. *Science (80-.).* **326**, 1086–1089 (2009).
50. Fontecilla-Camps, J. C. Nickel and the origin and early evolution of life. *Metallomics* **14**, (2022).
51. Diederich, P. *et al.* Nickel-organo compounds as potential enzyme precursors under simulated early Earth conditions. *Commun. Chem.* **7**, 33 (2024).
52. Simonson, B. M. Origin and evolution of large Precambrian iron formations. in *Extreme depositional environments: mega end members in geologic time* (eds. Chan, M. A. & Archer, A. W.) vol. 370 0 (Geological Society of America, 2003).
53. Planavsky, N. J. *et al.* Widespread iron-rich conditions in the mid-Proterozoic ocean. *Nature* **477**, 448–451 (2011).
54. Taylor, K. G. & Konhauser, K. O. Iron in Earth Surface Systems: A Major Player in Chemical and Biological Processes. *Elements* **7**, 83–88 (2011).
55. Frey, P. A. & Reed, G. H. The Ubiquity of Iron. *ACS Chem. Biol.* **7**, 1477–1481 (2012).
56. Ozturk, S. F. & Sasselov, D. D. On the origins of life's homochirality: Inducing enantiomeric excess with spin-polarized electrons. *Proc. Natl. Acad. Sci.* **119**, e2204765119 (2022).
57. Ozturk, S. F., Liu, Z., Sutherland, J. D. & Sasselov, D. D. Origin of biological homochirality by crystallization of an RNA precursor on a magnetic surface. *Sci. Adv.* **9**, eadg8274 (2023).
58. Dunlop, D. J. & Arkani□Hamed, J. Magnetic minerals in the Martian crust. *J. Geophys. Res. Planets* **110**, (2005).
59. Levitt, M. & Lifson, S. Refinement of protein conformations using a macromolecular energy minimization procedure. *J. Mol. Biol.* **46**, 269–279 (1969).
60. Polo, S. E. & Jackson, S. P. Dynamics of DNA damage response proteins at DNA breaks: a focus on protein modifications. *Genes Dev.* **25**, 409–433 (2011).
61. Chen, T.-Y., Cheng, Y.-S., Huang, P.-S. & Chen, P. Facilitated Unbinding via

Multivalency-Enabled Ternary Complexes: New Paradigm for Protein–DNA Interactions. *Acc. Chem. Res.* **51**, 860–868 (2018).
62. Safieh, J. *et al.* A molecular mechanism for the “digital” response of p53 to stress. *Proc. Natl. Acad. Sci.* **120**, e2305713120 (2023).
63. Khatua, S. & Taraphder, S. In the footsteps of an inhibitor unbinding from the active site of human carbonic anhydrase II. *J. Biomol. Struct. Dyn.* **41**, 3187–3204 (2023).
64. Fransson, J. Vibrational origin of exchange splitting and ’ ’chiral-induced spin selectivity. *Phys. Rev. B* **102**, 235416 (2020).
65. Fransson, J. Charge and Spin Dynamics and Enantioselectivity in Chiral Molecules. *J. Phys. Chem. Lett.* **13**, 808–814 (2022).
66. Santra, K., Lu, Y., Waldeck, D. H. & Naaman, R. Spin Selectivity Damage Dependence of Adsorption of dsDNA on Ferromagnets. *J. Phys. Chem. B* **127**, 2344–2350 (2023).

Acknowledgments
We thank Dr. Reinat Nevo for help with microscopy experiments. RN acknowledges partial support from the US-AFSOR Grant FA9550-21-1-0418. JF acknowledges support from Vetenskapsrådet and Stiftelsen Olle Engkvist Byggmästare. NM acknowledges the support of the Israel Science Foundation (1388/22). PV acknowledges financial support from the Feinberg Graduate School, Weizmann Institute of Science.

Funding:

RN acknowledges partial support from the US-AFSOR Grant FA9550-21-1-0418.
JF acknowledges support from Vetenskapsrådet and Stiftelsen Olle Engkvist Byggmästare.
NM acknowledges the support of the Israel Science Foundation (1388/22).
PV acknowledges financial support from the Feinberg Graduate School, Weizmann Institute of Science.

Author contributions:

PV and RN designed research. PV, KS, NP, AG, QZ and JF performed research. OWK, LML and NM contributed new reagents or analytic tools. PV, KS, NP, JF and RN analyzed data. PV and RN wrote the paper.

Competing interests: Authors declare that they have no competing interests

Data and materials availability: The authors declare that the data supporting the findings of this study are available within the paper and its Supplementary Information files. Should any raw data files be needed in another format they are available from the corresponding authors upon reasonable request. Source data are provided with this paper.